

Efficiency calibrations of cylindrically bent transmission crystals in the 20 to 80 keV x-ray energy range

Csilla I. Szabo,¹ Uri Feldman,¹ Stephen Seltzer,¹ Lawrence T. Hudson,² Michelle O'Brien,² Hye-Sook Park,³ and John F. Seely^{4,*}

¹Artep Inc., 2922 Excelsior Springs Court, Ellicott City, Maryland 21042, USA

²National Institute of Standards and Technology, Gaithersburg, Maryland 20899, USA

³Lawrence Livermore National Laboratory, Livermore, California 94550, USA

⁴Naval Research Laboratory, Space Science Division, Washington, D.C. 20036, USA

*Corresponding author: john.seely@nrl.navy.mil

Received December 17, 2010; revised March 3, 2011; accepted March 10, 2011; posted March 15, 2011 (Doc. ID 139881); published April 6, 2011

Two quartz (10–11) crystals were cylindrically bent to a 25.4 cm radius of curvature and were mounted in identical Cauchois-type transmission spectrometers, and the crystal diffraction efficiencies were measured to 5% absolute accuracy using narrow bandwidth x-ray source fluences in the 20 to 80 keV energy range. The measured integrated reflectivity values were compared to calculations performed using a computational model that accounts for the diffraction geometry of the bent transmission crystal. These crystal calibrations enable the accurate measurement of absolute hard x-ray emission levels from laser-produced plasmas and other laboratory sources.

OCIS codes: 340.7480, 300.6560, 050.1940.

Transmission-type spectrometers have been developed to record the hard x-ray spectra from laboratory radiography and medical sources [1–3]. The spectrometer employs a cylindrically bent crystal in the Cauchois geometry [4], and the spectrometer geometric design has been optimized to record the emission from laser-produced plasma sources with high wavelength dispersion [5–7]. Accurate measurement of the hard x-ray spectral emission requires the calibration of the bent crystal, and in this Letter we report the calibration of two quartz (10–11) crystals to 5% absolute accuracy in the 20 to 80 keV energy range.

To our knowledge, these are the first such accurate bent crystal calibrations for a pointlike x-ray source using narrow bandwidth x-ray fluences. We note that synchrotron radiation beams cannot be used for such accurate calibrations because their angular divergence is small compared to the crystal's angular aperture, and for large source-to-crystal standoff distances, radioactive sources tend to be too weak for accurate calibrations in a reasonable time and, in addition, are sparse in the 20 to 80 keV energy range.

Although these calibrations are specific to one set of bent crystals, the calibration techniques developed here can be generally applied to any x-ray optical element, such as those used as absolute yield and spectroscopic diagnostics of laser-produced plasmas and other laboratory sources. By comparing the accurately measured diffraction efficiencies with a computational model that accounts for the geometry of the bent transmission crystal, it was found that the calculated efficiencies were larger by a factor of 2. By scaling the calculated efficiencies to the measured efficiencies, it is possible to calculate the efficiency of any crystal operating in any order with reliability that is sufficient for the design and optimization of hard x-ray spectrometers for wide-ranging applications.

The calibration setup is shown schematically in Fig. 1. Using the cylindrical coordinate system (R, θ, φ) with the

origin at the source, let $F(E, R, \theta, \varphi)$ be the number of photon/s with energy E in the energy interval dE per steradian that is incident on the crystal. Let $\varepsilon(E, R, \theta, \varphi)$ be the fraction of photons with energy E that is diffracted through the crystal at point (R, θ, φ) , commonly called the diffraction efficiency. Then

$$S(E) = C(E) \int_{\theta} \int_{\varphi} F(E, R, \theta, \varphi) \varepsilon(E, R, \theta, \varphi) d\theta d\varphi, \quad (1)$$

where $S(E)$ is the detector signal/s, $C(E)$ is the conversion factor from photons incident on the detector to detector signal, and the integrals are over the illuminated angular acceptance of the crystal for a given spectrum.

We assume that the crystal's angular aperture is sufficiently small so that the variation of F over the crystal area is negligible. This is valid because, for these calibrations, the source to crystal distance is 60 cm, the illuminated crystal height is 2 cm, the length of crystal diffracting each narrowband spectrum is less than 1 mm, and the source fluence was observed to be flat over these crystal angular apertures. Then Eq. (1) can be written

$$S(E) = C(E)F(E, R_c)\delta(E)(H_c/R_c), \quad (2)$$

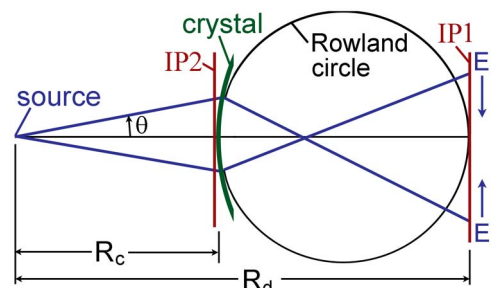


Fig. 1. (Color online) Schematic of the geometrical setup of the bent crystal (not to scale).

where H_c is the illuminated crystal height, R_c is the source to crystal distance, and

$$\delta(E) = \int_{\theta} \varepsilon(E, R_c, \theta) d\theta \quad (3)$$

is the diffraction efficiency integrated over the incidence angle θ (commonly called the integrated reflectivity), which depends on the crystal composition, orientation cut, bending radius, and thickness.

The integrated reflectivity is measured by taking the ratio of the detector signal generated by the photons diffracted by the crystal and the detector signal generated by the same photon distribution directly incident on the same detector placed at the crystal position. The latter signal is given by Eq. (2), with $\varepsilon(E, R, \theta, \varphi)$ equal to unity:

$$S_o(E) = C(E)F(E, R_c)(W_o/R_c)(H_o/R_c), \quad (4)$$

where H_o and W_o are the height and width of the detector area. From Eqs. (2) and (4), the integrated reflectivity is

$$\delta(E) = (W_o/R_c)(H_o/H_c)S(E)/S_o(E). \quad (5)$$

The integrated reflectivity is independent of the source distribution F and the detector sensitivity C , assuming the measurements with and without the crystal are performed using the same source conditions and the same detector, and this contributes to the high accuracy of the inferred integrated reflectivity.

The measurements were carried out using an x-ray source at the National Institute of Standards and Technology (NIST) having an electron-bombarded tungsten anode and producing a narrow photon energy distribution that is defined on the high energy end by the accurately controlled peak kilovoltage and on the low energy end by interchangeable filtration combinations [8]. The shapes of six photon distributions measured by a high purity germanium detector are shown in Fig. 2. These have been corrected for detector response and represent true photon spectra. Also indicated for each distribution is the average photon energy weighted by the intensity and the weighted standard deviation.

Two quartz crystals were calibrated, each cut by the same vendor with the (10–11) diffracting planes perpendicular to the surface and polished to 0.2 mm nominal thickness. Each crystal was bent onto a form having a 25.4 cm radius of curvature, and the image plate detector was placed on the Rowland circle at a distance of 25.4 cm from the crystal. The crystal was placed 60 cm from the

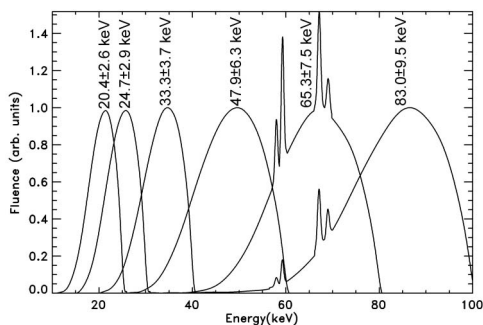


Fig. 2. Relative photon spectra of the six narrow bandpass fluences.

source, and the source to detector distance was therefore $R_d = 85.4$ cm. This detector, IP1 in Fig. 1, recorded the signal S in Eq. (5). When the crystal was removed, the image plate was placed at the crystal distance of $R_c = 60$ cm from the source, and this detector (IP2 in Fig. 1) measured the signal S_o in Eq. (5).

The detector was a Fuji BAS-MS image plate that was scanned by a Logos T100 scanner with 300 pixel steps per 2.54 cm. When placed behind the crystal on the Rowland circle, the spectral images recorded when using the source distributions having 24.7 and 65.3 keV average photon energies and 10 min exposure time are shown in Figs. 3(a) and 3(b). Each spectral image contains two mirror images dispersed on either side of the spectrometer's central axis with energy increasing toward the axis as indicated in Fig. 1 [3]. The lower portions of the images have filter K attenuation edges that were used to establish the (nonlinear) energy scales, where the filters were placed between the crystal and the image plate. Shown in Figs. 3(c) and 3(d) are the average signals in the horizontal (dispersion) direction, where the average is over rows in the upper portion of the spectral image without filter edges. Thus $S = (H_d/p)S_{\text{row}}$, where S_{row} is the average of pixel column values in the region of interest (ROI) summed over the narrow bandwidth photon spectrum, $p = 84.7 \mu\text{m}$ is the pixel row height, and H_d is the height of the ROI on the image plate over which the average row was calculated.

The direct exposures on the image plate placed at the crystal position required only 10 s exposure times. Thus, to account for fading of the latent image over the much longer exposure time when the image plate was behind the crystal (10 min), the procedure was to make two short exposures in front of the crystal, one long exposure behind the crystal, and two short exposures in front of the crystal, all on the same image plate. By comparing the readout counts from the first and last short exposures, it was possible to correct for the 4% to 5% fading that occurred during the 14 min required to complete and scan the five exposures.

Since the signal S is calculated from the average row of pixels spanning the spectrum recorded behind the crystal, the direct-exposure signal S_o recorded in front of the crystal was calculated from the average pixel value σ_o : $S_o = (W_o/p)(H_o/p)\sigma_o$. Thus Eq. (5) becomes

$$\delta = (pR_d/R_c^2)(S_{\text{row}}/\sigma_o) / \exp(-\mu(R_d - R_c)), \quad (6)$$

where the projection in the plane perpendicular to the dispersion plane is $H_d/H_c = R_d/R_c$ and the exponential factor accounts for the attenuation in air of the photons propagating from the crystal to the detector on the Rowland circle.

The absolute accuracy of the integrated reflectivity values is estimated by compiling the various possible uncertainties in the calibration procedures. Uncertainties in the image plate distances R_d and R_c are estimated to contribute less than 1%; x-ray source stability as monitored by a NIST free-air chamber detector, 0.1%; statistical variations in the Logos scanner values, 2%; uncertainty in the short duration (10 s) exposures, 2%; and averaging over the narrow bandwidth photon distributions, 2%,

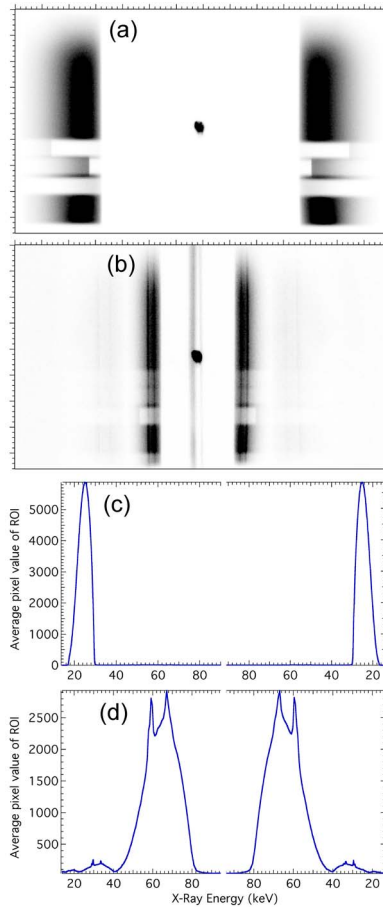


Fig. 3. (Color online) (a) and (b) are the spectral images recorded for the source fluences with average energies of 24.7 and 65.3 keV, and (c) and (d) are the average row spectra from the upper portions of the spectral images as functions of energy.

as estimated from the slope of the measured efficiency curve in Fig. 4 and the intensity-weighted energy intervals in Fig. 2. Considering that many of these uncertainties cancel out when the ratios of Eq. (6) are calculated, the estimated one-sigma relative uncertainties in the absolute values of the integrated reflectivity is 5%.

The data points in Fig. 4 show the first-order integrated reflectivity values δ of the two crystals measured on three experimental runs. Also shown is the ratio of the second and first orders measured for the three highest energies (second orders at the lower energies were beyond the range of observation; see Fig. 3). The values are in good agreement with relative variations of 2%, and this indicates the high precision of the measurements resulting from the stability of the x-ray source and to the repeatability of the image plate exposures and data analysis. In addition, this indicates that the integrated reflectivities of the two crystals, cut and polished by the same vendors, are identical within the experimental errors.

The curves in Fig. 4 are the integrated reflectivity values from a computational model that accounts for the geometry of the bent transmission crystal [9]. It was found that the best agreement with the measurements occurred for an effective crystal thickness of 0.1 mm,

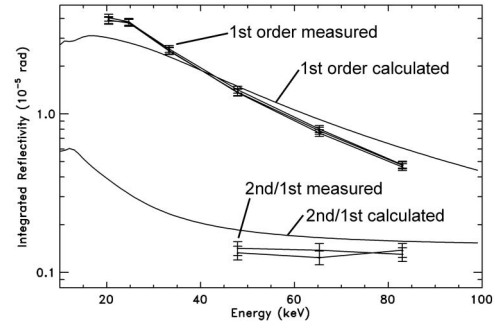


Fig. 4. Comparison of the first-order measured (data points) and calculated (curve) integrated reflectivities for the two crystals in units of 10^{-5} radians and the ratios of the second and first orders.

smaller than the 0.2 mm nominal thickness of the polished crystals. The resolution of this discrepancy will require further experimental and computational work, but, in any case, the scaled calculations can provide integrated reflectivity values that are sufficiently reliable for the optimization of bent crystals for various applications.

Having measured the integrated reflectivity of the bent crystal, and assuming the detector sensitivity $C(E)$ is known, the photon energy distributions incident on the crystal from laboratory sources can be measured using Eq. (2):

$$F(E, R_c) = S_{\text{row}}(R_d/p)/\delta(E)C(E), \quad (7)$$

where the bent crystal and the geometry are the same as for the calibration. Conversely, the detector sensitivity can be determined if the source distribution is known.

This work was supported Lawrence Livermore National Laboratory project B591129. The mention of commercial products does not imply endorsement by the U. S. Government or that they are necessarily the best for the application.

References

1. R. D. Deslattes, J. C. Levin, M. D. Walker, and A. Henins, *Med. Phys.* **21**, 123 (1994).
2. C. T. Chantler, R. D. Deslattes, A. Henins, and L. T. Hudson, *Br. J. Radiol.* **69**, 636 (1996).
3. L. T. Hudson, R. D. Deslattes, A. Henins, C. T. Chantler, E. G. Kessler, and J. E. Schewpe, *Med. Phys.* **23**, 1659 (1996).
4. Y. Cauchois, *J. Phys.* **3**, 320 (1932). English translation is available at <http://spectroscopy.nrl.navy.mil/>.
5. J. Seely, L. Hudson, G. Holland, and A. Henins, *Appl. Opt.* **47**, 2767 (2008).
6. H.-S. Park, B. Maddox, E. Giraldez, S. Hatchett, L. Hudson, N. Izumi, M. Key, S. Le Pape, A. MacKinnon, A. MacPhee, P. Patel, T. Phillips, B. Remington, J. Seely, R. Tommasini, R. Town, J. Workman, and E. Brambrink, *Phys. Plasmas* **15**, 072705 (2008).
7. J. Seely, C. Szabo, P. Audebert, E. Brambrink, E. Tabakhoff, and L. Hudson, *Phys. Plasmas* **17**, 023102 (2010).
8. P. Lamperti and M. O'Brien, "Calibration of x-ray and gamma-ray measuring instruments," NIST Special Publication 250 (2001).
9. Radcal Corporation, 426 West Duarte Road, Monrovia, Calif. 91016.